The Astrophysical Journal Letters, 924:L36 (5pp), 2022 January 10 https://doi.org/10.3847/2041-8213/ac447a

Superhorizon Perturbations: A Possible Explanation of the Hubble–Lemaître Tension and the Large-scale Anisotropy of the Universe

Prabhakar Tiwari[1], Rahul Kothari[2], and Pankaj Jain[3]
[1] National Astronomy Observatories, Chinese Academy of Science, Beijing 100101, People's Republic of China; ptiwari@nao.cas.cn
[2] Department of Physics & Astronomy, University of the Western Cape, Cape Town 7535, South Africa; quantummechanicskothari@gmail.com
[3] Department of Physics, Indian Institute of Technology, Kanpur-208016, India; pkjain@iitk.ac.in
Received 2021 November 23; accepted 2021 December 17; published 2022 January 18

Abstract

Current cosmological observations point to a serious discrepancy between the observed Hubble parameter obtained using direct versus cosmic microwave background radiation measurements. Besides this so-called Hubble–Lemaître tension, we also find considerable evidence in diverse cosmological observables that indicate violation of the cosmological principle. In this paper, we suggest that both these discrepancies are related and can be explained by invoking superhorizon perturbations in the universe. We implement this by considering a single superhorizon mode and showing that it leads to both a dipole in large-scale structures and a shift in the Hubble–Lemaître parameter. Furthermore, the shift is found to be independent of redshift up to a certain distance. This is nicely consistent with the data.

Unified Astronomy Thesaurus concepts: Large-scale structure of the universe (902); Dark matter (353); Inflationary universe (784); Hubble-Lemaitre law (763); Hubble constant (758)

1. Introduction

Around 90 yr ago, Georges Henri Joseph Édouard Lemaître proposed that an expanding universe can explain the recession of nearby galaxies (Lemaître 1927). With his expanding universe model, Lemaître derived the speed–distance relationship, "Hubble's Law,"[4] and estimated the rate of cosmic expansion, i.e., the "Hubble constant," equal to 645 km s^{-1} Mpc^{-1} (Peebles 1984; van den Bergh 2011; Way & Nussbaumer 2011). He did this by combining Gustaf Strömberg's redshift data (Stromberg 1925, who relied mostly on Vesto Slipher's work, Slipher 1917a) and Hubble's distances which were extracted using magnitudes (Hubble 1926; Way & Nussbaumer 2011). Soon after, Edwin Powell Hubble published his famous paper (Hubble 1929) where he and his assistant, Milton Humason used better stellar distance indicators such as Cepheid variables, novae, and velocities. The velocity information was primarily extracted from the spectroscopic Doppler-shift observations due to Vesto Melvin Slipher (Slipher 1917b). This established a linear relationship between velocity and distance and determined the value for the cosmic expansion term, the Hubble constant, equal to 500 km s^{-1} Mpc^{-1}. Hubble's remarkable observational relationship and the Hubble constant value were obtained using only 24 nearby galaxies for which both measured velocities and distances were available with certain accuracy. Shortly after Lemaître and Hubble's discovery, cosmologists, including Einstein, became aware that far away objects are moving faster than nearer ones and thus the expanding universe model was established.

The theoretical and observational advances of cosmology have confirmed a dark and exotic universe that is well described by the Friedman–Lemaître–Robertson–Walker (FLRW) metric (Friedmann 1922, 1924; Lemaître 1931, 1933; Robertson 1935, 1936a, 1936b; Walker 1937), consisting of ≈70% dark energy (Λ), ≈25% cold dark matter (CDM), and with only ≈5% familiar baryonic matter. Presently, the standard ΛCDM cosmological model that assumes zero spatial curvature ($\Omega_k = 0$), together with isotropy and homogeneity, provides the simplest explanation of our universe. It provides a good fit to a large number of cosmological observations, such as the CMB radiation, primordial helium abundance, baryonic acoustic oscillations (BAO), galaxy clustering, and Hubble parameter measurements etc.

Inspite of all these successes, there have been several different observations showing significant tension with the standard ΛCDM. In particular, the "direct" measurements of the Hubble–Lemaître parameter show a clear mismatch from ones observed using "indirect" CMB measurements. Most notably, the recent direct measurement of the Hubble–Lemaître parameter from Supernovae H0 for the Equation of State (SH0ES) collaboration, which uses Cepheid-calibrated SNIa, yields $H_0 = 73.5 \pm 1.4$ km s^{-1} Mpc^{-1} (Reid et al. 2019). To the contrary, the Planck satellite, using its precise CMB radiation fluctuation measurements (Planck Collaboration et al. 2020) finds $H_0 = 67.36 \pm 0.54$ km s^{-1} Mpc^{-1}. These two disagree with each other at 4.2σ (Anchordoqui & Perez Bergliaffa 2019) and this disagreement is widely known as Hubble–Lemaître tension in the literature (see, however, Rameez & Sarkar 2021 for a contrary view). For a review on the Hubble–Lemaître tension, see Di Valentino et al. (2021), Efstathiou (2020), and Di Valentino et al. (2021).

There have been several simultaneous attempts to calculate the H_0 value using direct and indirect methods. Indirect methods usually employ CMB or Big Bang nucleosynthesis with galaxy clustering measurements, viz. the Sloan Digital Sky Survey: Baryon Oscillation Spectroscopic Survey (BOSS) and the extended Baryon Oscillation Spectroscopic Survey. They produce a Hubble–Lemaître parameter value roughly in agreement with the aforementioned Planck satellite value (Aiola et al. 2020; Pogosian et al. 2020; Alam et al. 2021). By contrast, direct measurements, now extending across kpc to

[4] Now called the "Hubble–Lemaître Law."

Gpc scales, include observations from cepheids–SNIa (Riess et al. 2021), tip of the red-giant branch (TRGB)–SNIa (Reid et al. 2019), Miras–SNIa (Huang et al. 2020), masers (Pesce et al. 2020), surface brightness fluctuations (Blakeslee et al. 2021), the Tully–Fisher relation (Kourkchi et al. 2020), and gravitational waves (Gayathri et al. 2020; Mukherjee et al. 2020), are roughly in agreement with SH0ES observations. The direct measurements also include observations of lensing systems—for example, the H0 Lenses in COSMOGRAIL's Wellspring (H0LiCOW) collaboration (Wong et al. 2020) finds $H_0 = 73.3^{+1.7}_{-1.8}$ km s^{-1} Mpc^{-1}. Additionally, the Carnegie–Chicago Hubble Program, based on a calibration of TRGB applied to SNIa (Freedman et al. 2019), finds a somewhat lower value of the Hubble–Lemaître parameter equal to 69.8 ± 1.9 km s^{-1} Mpc^{-1}. Ever since the Hubble–Lemaître discovery, numerous extreme precision measurements of the Hubble–Lemaître parameter have been carried out. Over decades and to ever increasing distances, a variety of probes, such as SNIa standard candles (Schmidt et al. 1998; Riess et al. 1998; Perlmutter et al. 1999; Kirshner 2004; Betoule et al. 2014) and improved stellar/Cepheid distance indicators (Freedman et al. 2001), have been employed to achieve this. These advancements have made the directly measured value of the Hubble parameter extremely accurate—from Hubble's value of $H_0 = 500$ km s^{-1} Mpc^{-1} to the present value $H_0 = 73 \pm \sim 2$ km s^{-1} Mpc^{-1}. This has allowed us to make a close comparison between the CMB-derived H_0 value and the one from direct measurements.

To resolve this conflict between directly and indirectly measured H_0 values, there has been a flurry of proposals in the literature (see Schöneberg et al. 2021; Di Valentino et al. 2021 for a review of various solutions). These papers present various novel approaches such as the modification of dark energy (Karwal & Kamionkowski 2016; Alexander & McDonough 2019; Poulin et al. 2019; Berghaus & Karwal 2020; Bisnovatyi-Kogan 2020; Choi et al. 2020; Sakstein & Trodden 2020; Smith et al. 2020; Ye & Piao 2020; Panpanich et al. 2021), introduction of nonstandard neutrino interaction terms (Blinov et al. 2019; Escudero & Witte 2020; Escudero Abenza & Witte 2020; Ghosh et al. 2020; He et al. 2020; Kreisch et al. 2020), introduction of the fifth force (Desmond et al. 2019), emerging spatial curvature on account of nonlinear relativistic evolution (Bolejko 2018), modification of the theory of gravity (Shimon 2020; Vishwakarma 2020; Abadi & Kovetz 2021; Gurzadyan & Stepanian 2021), and modification of the ΛCDM by changing or adding energy components to it (Mörtsell & Dhawan 2018; Lin et al. 2019; Kaya 2020).

In addition to the Hubble–Lemaître tension, there exist other observations that also suggest a potential departure from the ΛCDM model. Some of these challenge the basic foundations of the model—the cosmological principle. These include dipole anisotropy in radio polarization offset angles (Jain & Ralston 1999), alignment of the CMB quadrupole and octopole (de Oliveira-Costa et al. 2004; Copi et al. 2015; Aluri et al. 2017), alignment of quasar polarizations (Hutsemékers 1998), dipole anisotropy in radio source counts (Singal 2011; Gibelyou & Huterer 2012; Rubart & Schwarz 2013; Tiwari et al. 2015; Tiwari & Nusser 2016; Colin et al. 2017; Bengaly et al. 2018), radio polarizations (Tiwari & Jain 2015), and bulk flow in X-ray clusters (Kashlinsky et al. 2010). Remarkably, all these indicate a preferred direction close to the observed CMB dipole (Ralston & Jain 2004). A recent study claims a dipole signal in quasar source counts at infrared frequencies which shows a deviation from the expected CMB dipole at the 4.9σ level (Secrest et al. 2021). Several claims of anisotropy in the Hubble constant also exist (Biermann 1976; Wiltshire et al. 2013; Luongo et al. 2021; Migkas et al. 2021). These observations suggest a potential departure from isotropy on the largest distance scales. A comprehensive discussion of such isotropy violations is given in Perivolaropoulos & Skara (2021).

In this Letter, we suggest that the two problems, i.e., (a) Hubble–Lemaître tension and (b) the observed violation of isotropy at large distance scales are related. We propose a novel and elegant solution to both problems with a minimal modification of the ΛCDM model.

2. A New Proposal to Relax Hubble–Lemaître Tension

In the late 1970s, Grishchuk & Zel'dovich (Grishchuk & Zeldovich 1978a, 1978b) pointed out that long wavelength, i.e., superhorizon perturbations to the metric could be significant without contradicting the observed temperature power spectrum of CMB. Such perturbations can explain the alignment of low-multipole moments of CMB (Gordon et al. 2005). We also have constraints on amplitudes and wavelengths of superhorizon perturbations from low-multipole moments of CMB (Smoot et al. 1991; Hinshaw et al. 2003).

To explain the implementation of superhorizon modes, we consider the conventional conformal Newtonian gauge with the scalar perturbation to the flat FLRW metric given as,

$$ds^2 = -(1 + 2\Psi)dt^2 + a^2(t)(1 - 2\Phi)\delta_{ij}dx^i dx^j, \quad (1)$$

where $a(t)$ is the usual cosmological scale factor with $a_0 = 1$. The perturbation Ψ to the temporal part of the metric corresponds to the Newtonian potential. The scalar Φ is the perturbation to the spatial curvature. In the absence of anisotropic stress, $\Psi = \Phi$. A single adiabatic superhorizon mode perturbation, providing initial conditions for Ψ, in its simplest form can be modeled as (Erickcek et al. 2008; Ghosh 2014; Das et al. 2021),

$$\Psi_p = \alpha \sin(\kappa x_3 + \omega), \quad (2)$$

where the subscript "p" is an abbreviation for primordial, α is the superhorizon mode amplitude, x_3 is the third component of the comoving position vector, κ being the magnitude of the wave vector $\boldsymbol{k}$, and ω is a constant phase factor. Also, we have fixed the coordinate such that the wave vector $\boldsymbol{k} = \kappa\hat{x}_3$. This kind of simple superhorizon mode has been shown to significantly affect the large-scale distribution of matter and can potentially explain (Ghosh 2014; Das et al. 2021) the puzzling excess dipole signal observed in radio galaxy distribution (Singal 2011; Gibelyou & Huterer 2012; Rubart & Schwarz 2013; Tiwari et al. 2015; Tiwari & Jain 2015; Tiwari & Nusser 2016; Colin et al. 2017) while simultaneously explaining the alignment of CMB quadrupole and octopole (Gordon et al. 2005). The superhorizon mode in Equation (2) introduces a perturbation to the gravitational potential between distant galaxies and us. This effectively introduces corrections to observed redshifts of galaxies. Das et al. (2021) show that a galaxy at redshift z in the presence of a superhorizon perturbation Ψ_p will be observed at redshift z_{obs}, such that

$$1 + z_{obs} = (1 + z)(1 + z_{Doppler})(1 + z_{grav}), \quad (3)$$

where $z_{\rm Doppler}$ and $z_{\rm grav}$ are, respectively, the redshifts due to our velocity relative to large-scale structure and potential perturbations introduced by superhorizon mode. The $z_{\rm obs}$ can be expanded and the leading monopole and dipole term can be written as,

$$z_{\rm obs} = \bar{z} + \gamma \cos\theta + ..., \tag{4}$$

Here θ is the polar angle of the spherical polar coordinate system, $\gamma \equiv \gamma(z, \alpha, \kappa, \omega)$ and is small in comparison with $\bar{z}$, the monopole term. The monopole term $\bar{z}$, given in Das et al. (2021), is

$$z_{\rm obs} \approx \bar{z} = z + (1+z)[g(z) - g(0)]\alpha \sin\omega, \tag{5}$$

where $g(z)$ represents the redshift evolution of $\Psi(z)$ such that $\Psi(z) = g(z)\Psi_{\rm p}$.

Ghosh (2014) and Das et al. (2021) successfully explain excess dipole signal observed with high-redshift galaxies (Singal 2011; Gibelyou & Huterer 2012; Rubart & Schwarz 2013; Tiwari et al. 2015; Tiwari & Jain 2015; Tiwari & Nusser 2016; Colin et al. 2017) using superhorizon perturbations. They find that a superhorizon mode, for a range of α, κ values, can consistently explain both the CMB and NVSS observations while remaining in harmony with others vis-à-via the dipole anisotropy in local Hubble–Lemaître parameter measurements and local bulk flow observations. Das et al. (2021) note that the phase $\omega = \pi$ conventionally maximizes the dipole signal in radio galaxies. They also provide sufficient details regarding superhorizon perturbations and their applications to galaxy clustering, Hubble–Lemaître parameter anisotropy measurements, bulk flow, etc. In addition to this, they find a monopole contribution which is nonzero as long as the phase $\omega \neq \pi$. The choice $\omega = \pi$ is rather special and implies that we have a preferred position in the universe. There is no physical motivation for this and here we explore the implications of the monopole term. Remarkably, we find that the monopole term in Equation (5) potentially solves the Hubble–Lemaître tension. We consider general values of phase ω and obtain the redshift monopole term in Equation (5). The Hubble–Lemaître law (for nearby galaxies) is written as,

$$V_{\rm obs} = H_0^{\rm obs} d, \tag{6}$$

where $V_{\rm obs}$ is the observed radial velocity of a galaxy at the proper distance d and $H_0^{\rm obs}$ is the observed Hubble–Lemaître parameter, corresponding to the observed redshift $z_{\rm obs}$. Thus we have (assuming $z_{\rm obs} \ll 1$)

$$z_{\rm obs} = \frac{V_{\rm obs}}{c} = \frac{d}{c(H_0^{\rm obs})^{-1}}. \tag{7}$$

Analogously, in the equation for redshift z, $V_{\rm obs}$ and $H_0^{\rm obs}$ would, respectively, be replaced by V and H_0. Here H_0 is the Hubble–Lemaître parameter predicted from CMB measurements.

We note that the velocity measurements are carried out using Doppler shift and thus the apparent change in z results in a change in velocity. This eventually leads to a change in the distance–velocity relation slope, i.e., Hubble–Lemaître parameter value. Therefore, if the observed redshifts $z_{\rm obs}$ differ z by 10%, the directly measured value $H_0^{\rm obs}$ will also differ from H_0 by the same amount. As the Hubble–Lemaître tension is all about $\sim$10% excess in directly measured Hubble–Lemaître parameter value, we seek this change in the redshift dipole term given in Equation (5). We find that a superhorizon mode with a range of α, κ, and ω values can consistently explain the excess galaxy dipole and Hubble–Lemaître tension. The set of values of these parameters is consistent with CMB, local bulk flow, and local redshift anisotropy limit.

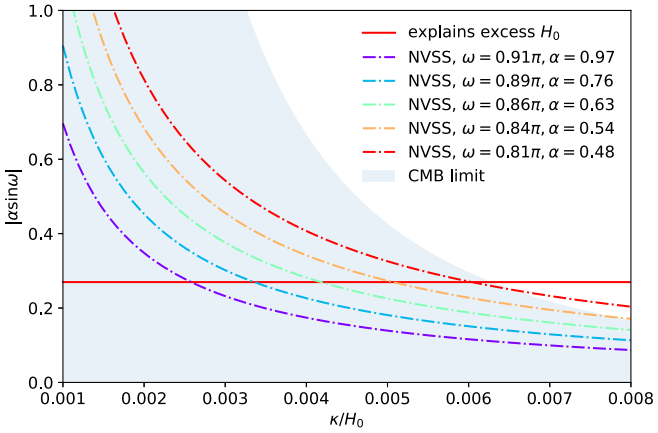

Figure 1. Plot of $|\alpha \sin\omega|$ vs. κ/H_0 for the observed Hubble–Lemaître tension and NVSS dipole amplitude for various values of ω. We have assumed a dipole amplitude equal to 0.0151 (Tiwari et al. 2015). The horizontal line satisfies the results of Reid et al. (2019), i.e., $H_0^{\rm obs} = 73.5$ km s^{-1} Mpc^{-1} at 7.57 Mpc, and the dotted dashed curves represent the NVSS excess dipole solution in the κ, α plane with different values of phase ω. The blue shaded part denotes the region of parameter space that satisfies the CMB quadrupole constraint (Erickcek et al. 2008). Note that for the κ range we have explored, and phase, $\omega \neq \pi$, only the quadrupole constraints turn out to be relevant.

Table 1
Some Possible Superhorizon Modes $\Psi_{\rm p}$ with Appropriate Parameters Simultaneously Satisfying the Results of Reid et al. (2019), i.e., $H_0^{\rm obs} = 73.5$ km s^{-1} Mpc^{-1} at 7.57 Mpc, and NVSS Excess Dipole

Superhorizon mode	ω	α	$\frac{\kappa}{H_0}$
1.	0.91π	0.97	2.581×10^{-3}
2.	0.89π	0.76	3.357×10^{-3}
3.	0.86π	0.63	4.180×10^{-3}
4.	0.84π	0.54	5.067×10^{-3}
5.	0.81π	0.48	6.037×10^{-3}

2.1. Possible Values of Parameters

We consider the work of Reid et al. (2019) and produce the Hubble–Lemaître measurements considering superhorizon perturbation mode. The details of the fitting procedure are given in the Appendix. The results are shown in Figure 1. Some possible sets of values of α, κ, and ω, which simultaneously explain the dipole from NRAO VLA Sky Survey (NVSS) data[5] and the Hubble–Lemaître measurements are listed in Table 1. In general, a superhorizon mode with a phase ω, with a "reasonable" amplitude α and wavelength $2\pi/\kappa$, can explain excess NVSS dipole and Hubble–Lemaître tension. Furthermore, it is also noted that for a given superhorizon mode, the apparent Hubble–Lemaître parameter roughly remains the same for a very wide range of distances. The variation of $H_0^{\rm obs}$ with distance is given in Figure 2. We add that superhorizon modes

[5] et al. 2015), and we have considered the number density, $N(z) \propto z^{0.74} \exp\left[-\left(\frac{z}{0.71}\right)^{1.06}\right]$, and galaxy bias $b(z) = 0.33z^2 + 0.85z + 1.6$ (Nusser & Tiwari 2015; Tiwari & Nusser 2016). We impose an upper redshift cutoff in the abundance of sources at $z = 3.5$. Note that this redshift cutoff in reference Das et al. (2021) is $z = 2$.

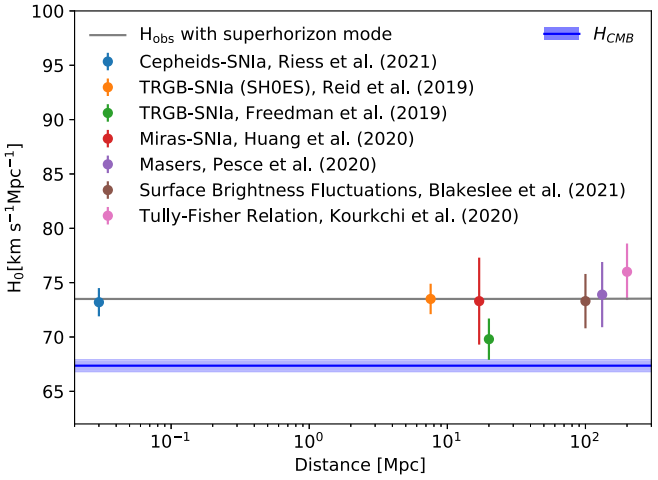

Figure 2. Apparent value of Hubble–Lemaître parameter with direct measurements at different distances. It is noted that the directly measured Hubble–Lemaître parameter remains roughly the same from distance as small as kpc to hundreds of Mpc. The Hubble–Lemaître measurements (data points) are obtained by combining many objects, the distance (x-axis) shown in figure corresponds to far most object used for analysis. All data points except CMB are direct measurements of Hubble–Lemaître parameter.

with CMB limits along with the NVSS dipole solution curve are consistent with local Hubble dipole and bulk flow observations (Das et al. 2021).

3. Conclusion and Outlook

Current cosmological observations suggest two discrepancies with the ΛCDM model. These are the Hubble–Lemaître tension and the large-scale anisotropy of the universe. With more observations, these discrepancies have only grown stronger. In this paper, we have shown that both of these can be explained within the framework of a phenomenological model that assumes the existence of a superhorizon mode in the universe. Such a mode is consistent with all existing cosmological observations and is already known to explain the CMB quadrupole–octopole alignment and the excess dipole in large-scale structures. It is therefore quite fascinating that it can also explain the Hubble–Lemaître tension, which a priori appears to be a completely independent phenomenon. The model introduces only three new parameters, namely the amplitude, wavelength, and the phase of the mode. Besides this, no special fine tuning of parameters is required for fitting the observables. This leads to a Hubble parameter that is approximately constant up to distances of order a few hundred Mpc, which is nicely consistent with observations. The model is likely to make a wide range of cosmological predictions which can be tested in future. In particular, it will induce a small anisotropy along with a correlated isotropic shift in several other cosmological observables, such as BAO and the epoch of reionization, besides Hubble constant. At large redshifts, the model predicts an interesting redshift dependence, which can also be tested in future studies (Das et al. 2021); this unique feature can potentially provide strong evidence for the existence of superhorizon modes.

Theoretically, such a superhorizon mode may arise as a stochastic phenomenon, called spontaneous breakdown of isotropy (Gordon et al. 2005). In this case it would be consistent with the cosmological principle. Another interesting possibility is that it may arise from an early phase of inflation. Inflation provides the only known theoretical explanation for the observed isotropy and homogeneity of the universe. Since we do not so far know how the universe originated, it is natural to assume that at some early time it may be described by an unknown inhomogeneous and anisotropic metric. During inflation, and essentially independent of the initial conditions, the metric becomes almost identical to the standard FLRW metric, possibly within one e-fold (Wald 1983). During such an early phase, when the universe had not yet acquired its cherished properties of isotropy and homogeneity, it could have generated modes that do not obey the cosmological principle (Rath et al. 2013). Furthermore, a wide range of parameters for which these modes can affect observations exist today (Aluri & Jain 2012). Hence, these observations, which appear to show deviations from ΛCDM, might offer a glimpse into a so far obscure early phase of the universe and may be consistent with the Big Bang paradigm (Rath et al. 2013).

P.T. acknowledges support from the National Key Basic Research and Development Program of China (No. 2018YFA0404503), NSFC grants 11925303 and 11720101004, and a grant from the CAS Interdisciplinary Innovation Team. R.K. is supported by the South African Radio Astronomy Observatory and the National Research Foundation (grant No. 75415).

Appendix
Procedure

In this Appendix we provide the details of the procedure used to fit the Hubble constant and the NVSS dipole. Using Equation (5), we get

$$\alpha \sin\omega = \frac{\delta z/z}{(1/z+1)\Delta g(z)}, \tag{A1}$$

where $\delta z = z_{\rm obs} - z$ and $\Delta g(z) = g(z) - g(0)$. Further, using Equation (7) it can be shown that $\delta z/z = \delta H_0/H_0$, with $\delta H_0 = H_0^{\rm obs} - H_0$.

From Reid et al. (2019) and Planck Collaboration et al. (2020), we have $H_0^{\rm obs} = 73.5\ {\rm km\ s^{-1}\ Mpc^{-1}}$ at 7.57 Mpc and $H_0 = 67.36\ {\rm km\ s^{-1}\ Mpc^{-1}}$. This gives $\delta H_0/H_0 = 0.0911$. Following standard ΛCDM and cosmological parameters from Planck 2018 results (Planck Collaboration et al. 2020), the proper distance $d = 7.57$ Mpc corresponds to $z = 0.0017$. So we set $\delta z/z = 0.0911$ with $z = 0.0017$ in Equation (A1) and obtain $\alpha \sin\omega = 0.2697$. This value corresponds to the red solid line of Figure 1, satisfying the Reid et. al. Hubble–Lemaître parameter observation.

In addition to the above condition, parameters α and ω are also constrained by CMB quadrupole and octopole values (Erickcek et al. 2008),

$$|\alpha_{\rm dec} \sin\omega| \leqslant 5.8\mathcal{Q}/(\kappa\chi_{_{\rm dec}})^2, \tag{A2}$$

$$|\alpha_{\rm dec} \cos\omega| \leqslant 32\mathcal{O}/(\kappa\chi_{_{\rm dec}})^3, \tag{A3}$$

where subscript "dec" denotes the parameters at decoupling, $\Psi_{\rm dec} = 0.937\Psi_p$ (Erickcek et al. 2008), and thus $\alpha_{\rm dec} = 0.937\alpha$. $\chi_{_{\rm dec}}$ is the comoving distance to decoupling, and $\mathcal{Q}$ and $\mathcal{O}$ are three times the measured rms values of the CMB quadrupole and octopole, respectively (Erickcek et al. 2008). We use the latest Planck Collaboration et al. (2020) values of $Q = 3\sqrt{C_2} \leqslant 1.69 \times 10^{-5}$ and $\mathcal{O} = 3\sqrt{C_3} \leqslant 2.44 \times 10^{-5}$. Following Equation (A2), we obtain the CMB limit on $|\alpha \sin\omega|$, i.e., the blue shaded region of Figure 1. To explain Reid et al.'s (2019) excess H_0, we impose (a) $\alpha \sin\omega = 0.2697$ and (b) CMB limits. Using these, we find $\kappa/H_0 \leqslant 6.29 \times 10^{-3}$.

The NVSS galaxies extend over the redshift range $z = 0$ to 3.5 (Nusser & Tiwari 2015; Tiwari & Nusser 2016). We note from Das et al. (2021) that to obtain the NVSS dipole as a consequence of the superhorizon mode,

$$\alpha \cos \omega = \frac{H_0}{\kappa} \frac{\mathcal{D}_{\rm obs} - \mathcal{B}}{\mathcal{A}_1(0,\, 3.5) + \mathcal{A}_2(0,\, 3.5) + \mathcal{C}(0,\, 3.5)}, \quad \text{(A4)}$$

where $\mathcal{D}_{\rm obs}$ is the observed NVSS dipole. Other terms in Equation (A4) are defined in Das et al. (2021). To obtain $\alpha \sin \omega$ versus κ/H_0 curves (dashed–dotted curves in Figure 1) satisfying NVSS dipole, we multiply Equation (A4) by $\tan \omega$ after choosing a specific phase ω. For the allowed κ range, the value of $\alpha \cos \omega$ needed to explain excess NVSS dipole in Equation (A4) is much less than the octopole limit in Equation (A3).

The intersection points of red solid line and NVSS curves in Figure 1 are the possible solutions to explain both Hubble–Lemaître tension and NVSS excess dipole. The parameters for these superhorizon modes are listed in Table 1.

In Figure 2, we fix $\alpha \sin \omega$ to satisfy Reid et al. (2019) Hubble–Lemaître parameter value and then calculate $H_0^{\rm obs}$ predicted with superhorizon mode from data at different distances (redshifts) using Equation (A1).

ORCID iDs

Prabhakar Tiwari https://orcid.org/0000-0001-7888-4270
Rahul Kothari https://orcid.org/0000-0003-1434-2418
Pankaj Jain https://orcid.org/0000-0001-8181-5639

References

Abadi, T., & Kovetz, E. D. 2021, PhRvD, 103, 023530
Aiola, S., Calabrese, E., Maurin, L., et al. 2020, JCAP, 2020, 047
Alam, S., Aubert, M., Avila, S., et al. 2021, PhRvD, 103, 083533
Alexander, S., & McDonough, E. 2019, PhLB, 797, 134830
Aluri, P. K., & Jain, P. 2012, MPLA, 27, 50014
Aluri, P. K., Ralston, J. P., & Weltman, A. 2017, MNRAS, 472, 2410
Anchordoqui, L. A., & Perez Bergliaffa, S. E. 2019, PhRvD, 100, 123525
Bengaly, C. A. P., Maartens, R., & Santos, M. G. 2018, JCAP, 04, 031
Berghaus, K. V., & Karwal, T. 2020, PhRvD, 101, 083537
Betoule, M., Kessler, R., Guy, J., et al. 2014, A&A, 568, A22
Biermann, P. 1976, A&A, 53, 295
Bisnovatyi-Kogan, G. S. 2020, arXiv:2002.05602
Blakeslee, J. P., Jensen, J. B., Ma, C.-P., Milne, P. A., & Greene, J. E. 2021, ApJ, 911, 65
Blinov, N., Kelly, K. J., Krnjaic, G. Z., & McDermott, S. D. 2019, PhRvL, 123, 191102
Bolejko, K. 2018, PhRvD, 97, 103529
Choi, G., Suzuki, M., & Yanagida, T. T. 2020, PhLB, 805, 135408
Colin, J., Mohayaee, R., Rameez, M., & Sarkar, S. 2017, MNRAS, 471, 1045
Copi, C. J., Huterer, D., Schwarz, D. J., & Starkman, G. D. 2015, MNRAS, 449, 3458
Das, K. K., Sankharva, K., & Jain, P. 2021, JCAP, 2021, 035
de Oliveira-Costa, A., Tegmark, M., Zaldarriaga, M., & Hamilton, A. 2004, PhRvD, 69, 063516
Desmond, H., Jain, B., & Sakstein, J. 2019, PhRvD, 100, 043537
Di Valentino, E., Anchordoqui, L. A., Akarsu, Ö., et al. 2021, APh, 131, 102605
Di Valentino, E., Mena, O., Pan, S., et al. 2021, CQGra, 38, 153001
Efstathiou, G. 2020, arXiv:2007.10716
Erickcek, A. L., Carroll, S. M., & Kamionkowski, M. 2008, PhRvD, 78, 083012
Escudero Abenza, M., & Witte, S. J. 2020, arXiv:2004.01470
Escudero, M., & Witte, S. J. 2020, EPJC, 80, 294
Freedman, W. L., Madore, B. F., Gibson, B. K., et al. 2001, ApJ, 553, 47
Freedman, W. L., Madore, B. F., Hatt, D., et al. 2019, ApJ, 882, 34
Friedmann, A. 1922, ZPhy, 10, 377
Friedmann, A. 1924, ZPhy, 21, 326
Gayathri, V., Healy, J., Lange, J., et al. 2020, arXiv:2009.14247
Ghosh, S. 2014, PhRvD, 89, 063518
Ghosh, S., Khatri, R., & Roy, T. S. 2020, PhRvD, 102, 123544
Gibelyou, C., & Huterer, D. 2012, MNRAS, 427, 1994
Gordon, C., Hu, W., Huterer, D., & Crawford, T. M. 2005, PhRvD, 72, 103002
Grishchuk, L. P., & Zeldovich, I. B. 1978a, AZh, 55, 209
Grishchuk, L. P., & Zeldovich, I. B. 1978b, SvA, 22, 125
Gurzadyan, V. G., & Stepanian, A. 2021, EPJP, 136, 235
He, H.-J., Ma, Y.-Z., & Zheng, J. 2020, JCAP, 11, 003
Hinshaw, G., Spergel, D. N., Verde, L., et al. 2003, ApJS, 148, 135
Huang, C. D., Riess, A. G., Yuan, W., et al. 2020, ApJ, 889, 5
Hubble, E. 1929, Proceedings of the National Academy of Sciences, 15, 168
Hubble, E. P. 1926, ApJ, 64, 321
Hutsemékers, D. 1998, A&A, 332, 410
Jain, P., & Ralston, J. P. 1999, MPLA, 14, 417
Karwal, T., & Kamionkowski, M. 2016, PhRvD, 94, 103523
Kashlinsky, A., Atrio-Barandela, F., Ebeling, H., Edge, A., & Kocevski, D. 2010, ApJL, 712, L81
Kaya, A. 2020, PhRvD, 101, 083523
Kirshner, R. P. 2004, Proceedings of the National Academy of Sciences, 101, 8
Kourkchi, E., Tully, R. B., Anand, G. S., et al. 2020, ApJ, 896, 3
Kreisch, C. D., Cyr-Racine, F.-Y., & Doré, O. 2020, PhRvD, 101, 123505
Lemaître, G. 1927, ASSB, 47, 49
Lemaître, G. 1931, MNRAS, 91, 483
Lemaître, G. 1933, ASSB, 53, 51
Lin, M.-X., Benevento, G., Hu, W., & Raveri, M. 2019, PhRvD, 100, 063542
Livio, M. 2011, Natur, 479, 171
Luongo, O., Muccino, M., Colgáin, E. O., Sheikh-Jabbari, M. M., & Yin, L. 2021, arXiv:2108.13228
Migkas, K., Pacaud, F., Schellenberger, G., et al. 2021, A&A, 649, A151
Mörtsell, E., & Dhawan, S. 2018, JCAP, 09, 025
Mukherjee, S., Ghosh, A., Graham, M. J., et al. 2020, arXiv:2009.14199
Nusser, A., & Tiwari, P. 2015, ApJ, 812, 85
Panpanich, S., Burikham, P., Ponglertsakul, S., & Tannukij, L. 2021, ChPhC, 45, 015108
Peebles, P. J. E. 1984, in The Big Bang and Georges Lemaître, ed. A. Berger (Dordrecht: Springer), 23
Perivolaropoulos, L., & Skara, F. 2021, arXiv:2105.05208
Perlmutter, S., Aldering, G., Goldhaber, G., et al. 1999, ApJ, 517, 565
Pesce, D. W., Braatz, J. A., Reid, M. J., et al. 2020, ApJL, 891, L1
Planck Collaboration, Aghanim, N., Akrami, Y., et al. 2020, A&A, 641, A6
Pogosian, L., Zhao, G.-B., & Jedamzik, K. 2020, ApJL, 904, L17
Poulin, V., Smith, T. L., Karwal, T., & Kamionkowski, M. 2019, PhRvL, 122, 221301
Ralston, J. P., & Jain, P. 2004, IJMPD, 13, 1857
Rameez, M., & Sarkar, S. 2021, CQGra, 38, 154005
Rath, P., Mudholkar, T., Jain, P., Aluri, P., & Panda, S. 2013, JCAP, 4, 7
Reid, M. J., Pesce, D. W., & Riess, A. G. 2019, ApJL, 886, L27
Riess, A. G., Casertano, S., Yuan, W., et al. 2021, ApJL, 908, L6
Riess, A. G., Filippenko, A. V., Challis, P., et al. 1998, AJ, 116, 1009
Robertson, H. P. 1935, ApJ, 82, 284
Robertson, H. P. 1936a, ApJ, 83, 187
Robertson, H. P. 1936b, ApJ, 83, 257
Rubart, M., & Schwarz, D. J. 2013, A&A, 555, A117
Sakstein, J., & Trodden, M. 2020, PhRvL, 124, 161301
Schmidt, B. P., Suntzeff, N. B., Phillips, M. M., et al. 1998, ApJ, 507, 46
Schöneberg, N., Franco Abellán, G., Pérez Sánchez, A., et al. 2021, arXiv:2107.10291
Secrest, N. J., Hausegger, S. V., Rameez, M., et al. 2021, ApJL, 908, L51
Shimon, M. 2020, arXiv:2012.10879
Singal, A. K. 2011, ApJL, 742, L23
Slipher, V. M. 1917a, PAPhS, 56, 403
Slipher, V. M. 1917b, Obs, 40, 304
Smith, T. L., Poulin, V., & Amin, M. A. 2020, PhRvD, 101, 063523
Smoot, G. F., Bennett, C. L., Kogut, A., et al. 1991, ApJL, 371, L1
Stromberg, G. 1925, ApJ, 61, 353
Tiwari, P., & Jain, P. 2015, MNRAS, 447, 2658
Tiwari, P., Kothari, R., Naskar, A., Nadkarni-Ghosh, S., & Jain, P. 2015, APh, 61, 1
Tiwari, P., & Nusser, A. 2016, JCAP, 2016, 062
van den Bergh, S. 2011, JRASC, 105, 151
Vishwakarma, R. G. 2020, IJMPD, 29, 2043025
Wald, R. M. 1983, PhRvD, 28, 2118R
Walker, A. G. 1937, Proc. London Math. Soc., 42, 90
Way, M., & Nussbaumer, H. 2011, PhT, 64, 8
Wiltshire, D. L., Smale, P. R., Mattsson, T., & Watkins, R. 2013, PhRvD, 88, 083529
Wong, K. C., Suyu, S. H., Chen, G. C. F., et al. 2020, MNRAS, 498, 1420
Ye, G., & Piao, Y.-S. 2020, PhRvD, 101, 083507